# Switchable single-dual-wavelength Yb,Na:CaF₂ waveguide lasers operating in continuous-wave and pulsed regimes

YINGYING REN,[1,2,6] CHEN CHENG,[3] YUECHEN JIA,[4] YANG JIAO,[1] DENGWANG LI,[1] MARK D. MACKENZIE,[5] AJOY K. KAR,[5] AND FENG CHEN[3,7]

[1]Center of light manipulations and applications, School of Physics and Electronics, Shandong Normal University, Jinan 250014, China
[2]Institute of Data Science and Technology, Shandong Normal University, Jinan 250014, China
[3]School of Physics, State Key Laboratory of Crystal Materials, Shandong University, Jinan 250100, China
[4]Laboratory for Optical Systems, Department of Microsystems Engineering - IMTEK, University of Freiburg, Georges-Köhler-Allee 102, 79110 Freiburg, Germany
[5]Institute of Photonics and Quantum Sciences, Heriot-Watt University, Edinburgh EH14 4AS, UK
[6]ryywly@sdnu.edu.cn
[7]drfchen@sdu.edu.cn

**Abstract:** Depressed-cladding waveguides are produced in a Yb,Na:CaF₂ laser crystal by applying an ultrafast laser inscription. Under pumping at 946 nm, continuous-wave (CW) and Q-switched laser oscillations with low thresholds are realized in these waveguide structures. With the variation of pumping power, switchable single- and dual-wavelength laser emissions peaking at 1013.9 nm and 1027.9 nm are generated. The maximum output power achieved for CW lasing is about 170 mW, corresponding to an optical-to-optical conversion efficiency as high as 45.3%. A pulse energy of 0.13 μJ is obtained for the waveguide laser operating in the pulsed regime.

## References and links

1. Y. Y. Ren, G. Brown, R. Mary, G. Demetriou, D. Popa, F. Torrisi, A. C. Ferrari, F. Chen, and A. K. Kar, "7.8-GHz Graphene-Based 2-μm Monolithic Waveguide Laser," IEEE J. Sel. Top. Quant. **21**(1), 1602106 (2015).
2. A. G. Okhrimchuk, A. V. Shestakov, I. Khrushchev, and J. Mitchell, "Depressed cladding, buried waveguide laser formed in a YAG:Nd³⁺ crystal by femtosecond laser writing," Opt. Lett. **30**(17), 2248–2250 (2005).
3. W. Nie, C. Cheng, Y. Jia, C. Romero, J. R. Vázquez de Aldana, and F. Chen, "Dual-wavelength waveguide lasers at 1064 and 1079 nm in Nd:YAP crystal by direct femtosecond laser writing," Opt. Lett. **40**(10), 2437–2440 (2015).
4. D. Choudhury, J. R. Macdonald, and A. K. Kar, "Ultrafast laser inscription: perspectives on future integrated applications," Laser Photonics Rev. **8**(6), 827–846 (2014).
5. F. Chen and J. R. Vázquez de Aldana, "Optical waveguides in crystalline dielectric materials produced by femtosecond laser micromachining," Laser Photonics Rev. **8**(2), 251–275 (2014).
6. A. Majkić, M. Zgonik, A. Petelin, M. Jazbinsek, B. Ruiz, C. Medrano, and P. Gunter, "Terahertz source at 9.4 THz based on a dual-wavelength infrared laser and quasi-phase matching in organic crystals OH1," Appl. Phys. Lett. **105**(14), 141115 (2014).
7. M. Scheller, J. M. Yarborough, J. V. Moloney, M. Fallahi, M. Koch, and S. W. Koch, "Room temperature continuous wave milliwatt terahertz source," Opt. Express **18**(26), 27112–27117 (2010).
8. K. Miyamoto, H. Minamide, M. Fujiwara, H. Hashimoto, and H. Ito, "Widely tunable terahertz-wave generation using an N-benzyl-2-methyl-4-nitroaniline crystal," Opt. Lett. **33**(3), 252–254 (2008).
9. T. Y. Fan, "Heat generation in Nd:YAG and Yb:YAG," IEEE J. Quantum Electron. **29**(6), 1457–1459 (1993).
10. A. Brenier, C. Y. Tu, Z. J. Zhu, and J. F. Li, "Dual-polarization and dual-wavelength diode-pumped laser operation from a birefringent Yb³⁺-doped GdAl₃(BO₃)₄ nonlinear crystal," Appl. Phys. B-Lasers and Optics **89**(2–3), 323–328 (2007).

11. H. Yoshioka, S. Nakamura, T. Ogawa, and S. Wada, "Dual-wavelength mode-locked Yb:YAG ceramic laser in single cavity," Opt. Express **18**(2), 1479–1486 (2010).
12. W. Ge, H. Liang, J. Ma, G. Xie, W. Gao, P. Yuan, L. Qian, X. Xu, and J. Xu, "Wavelength-switchable mode-locked Yb:LuAG laser between 1031 nm and 1046 nm," Opt. Express **22**(3), 2423–2428 (2014).
13. Q. Yang, Y. G. Wang, D. H. Liu, J. Liu, L. H. Zheng, L. B. Su, and J. Xu, "Dual-wavelength mode-locked Yb:LuYSiO$_5$ laser with a double- walled carbon nanotube saturable absorber," Laser Phys. Lett. **9**(2), 135–140 (2012).
14. X. J. Zhu, C. H. Wang, S. X. Liu, D. F. Hu, J. J. Wang, and C. Y. Zhu, "Switchable dual-wavelength and passively mode-locked all-normal-dispersion Yb-doped fiber lasers," IEEE Photonics Technol. Lett. **23**(14), 956–958 (2011).
15. V. Petit, P. Moretti, P. Camy, J.-L. Doualan, and R. Moncorgé, "Active waveguides produced in Yb$^{3+}$:CaF$_2$ by H$^+$ implantation for laser applications," J. Alloys Compd. **451**(1), 68–70 (2008).
16. M. Ams, P. Dekker, G. D. Marshall, and M. J. Withford, "Ultrafast laser-written dual-wavelength waveguide laser," Opt. Lett. **37**(6), 993–995 (2012).
17. J. Tu, S. A. FitzGerald, J. A. Campbell, and A. J. Sievers, "Glass-Like Properties Observed in Low-Frequency Raman Scattering of Mixed Fluorite Crystals," J. Non-Cryst. Solids **203**(96), 153–158 (1996).
18. F. Druon, S. Ricaud, D. N. Papadopoulos, A. Pellegrina, P. Camy, J. L. Doualan, R. Moncorgé, A. Courjaud, E. Mottay, and P. Georges, "On Yb:CaF$_2$ and Yb:SrF$_2$: review of spectroscopic and thermal properties and their impact on femtosecond and high power laser performance," Opt. Mater. Express **1**(3), 489–502 (2011).
19. A. Lucca, G. Debourg, M. Jacquemet, F. Druon, F. Balembois, P. Georges, P. Camy, J. L. Doualan, and R. Moncorgé, "High-power diode-pumped Yb$^{3+}$:CaF$_2$ femtosecond laser," Opt. Lett. **29**(23), 2767–2769 (2004).
20. G. Machinet, P. Sevillano, F. Guichard, R. Dubrasquet, P. Camy, J. L. Doualan, R. Moncorgé, P. Georges, F. Druon, D. Descamps, and E. Cormier, "High-brightness fiber laser-pumped 68 fs-2.3 W Kerr-lens mode-locked Yb:CaF$_2$ oscillator," Opt. Lett. **38**(20), 4008–4010 (2013).
21. M. Kowalczyk, A. Major, and J. Sotor, "High peak power ultrafast Yb:CaF$_2$ oscillator pumped by a single-mode fiber-coupled laser diode," Opt. Express **25**(21), 26289–26295 (2017).
22. J. Körner, J. Hein, H. Liebetrau, R. Seifert, D. Klöpfel, M. Kahle, M. Loeser, M. Siebold, U. Schramm, and M. C. Kaluza, "Efficient burst mode amplifier for ultra-short pulses based on cryogenically cooled Yb$^{3+}$:CaF$_2$," Opt. Express **21**(23), 29006–29012 (2013).
23. L. Su, J. Xu, H. Li, W. Yang, Z. Zhao, J. Si, Y. Dong, and G. Zhou, "Codoping Na$^+$ to modulate the spectroscopy and photoluminescence properties of Yb$^{3+}$ in CaF$_2$ laser crystal," Opt. Lett. **30**(9), 1003–1005 (2005).
24. H. T. Zhu, J. Liu, S. Z. Jiang, S. C. Xu, L. B. Su, D. P. Jiang, X. B. Qian, and J. Xu, "Diode-pumped Yb,Y:CaF$_2$ laser mode-locked by monolayer graphene," Opt. Laser Technol. **75**, 83–86 (2015).
25. J. L. Doualan, L. B. Su, G. Brasse, A. Benayad, V. Menard, Y. Y. Zhan, A. Braud, P. Camy, J. Xu, and R. Moncorge, "Improvement of infrared laser properties of Nd:CaF$_2$ crystals via codoping with Y$^{3+}$ and Lu$^{3+}$ buffer ions," J. Opt. Soc. Am. B **30**(11), 3018–3021 (2013).
26. J. F. Zhu, L. J. Zhang, Z. Y. Gao, J. L. Wang, Z. H. Wang, L. B. Su, L. H. Zheng, J. Y. Wang, J. Xu, and Z. Y. Wei, "Diode-pumped femtosecond mode-locked Nd, Y-codoped CaF$_2$ laser," Laser Phys. Lett. **12**(3), 035801 (2015).
27. J. Xu, L. B. Su, D. Zhang, J. Du, X. Y. Liang, Y. H. Xue, L. Chai, X. D. Xu, and G. J. Zhao, "Thermal, spectroscopic and laser properties of Yb$^{3+}$, Na$^+$:CaF$_2$ single crystals," J. Cryst. Growth **291**(1), 267–271 (2006).
28. L. Su, J. Xu, Y. Xue, C. Wang, L. Chai, X. Xu, and G. Zhao, "Low-threshold diode-pumped Yb$^{3+}$,Na$^+$:CaF$_2$ self-Q-switched laser," Opt. Express **13**(15), 5635–5640 (2005).
29. D. Marcuse, "Loss analysis of single-mode fiber splices," Bell Syst. Tech. J. **56**(5), 703–718 (1977).
30. C. Grivas, "Optically pumped planar waveguide lasers: Part II: Gain media, laser systems, and applications," Prog. Quantum Electron. **45–46**, 3–160 (2016).
31. W. P. Risk, "Modeling of longitudinally pumped solid-state lasers exhibiting reabsorption losses," J. Opt. Soc. Am. B **5**(7), 1412–1423 (1988).
32. C. Grivas, "Optically pumped planar waveguide lasers, part I: Fundamentals and fabrication techniques," Prog. Quantum Electron. **35**(6), 159–239 (2011).
33. T. Y. Fan and R. L. Byer, "Modeling and CW Operation of a Quasi-Three-Level 946 nm Nd: YAG Laser," IEEE J. Quantum Electron. **23**(5), 605–612 (1987).

## 1. Introduction

In past decades, many researchers have highlighted the merits of cladding waveguide geometries fabricated via Ultrafast Laser Inscription (ULI) in terms of flexibility and functionality for fabricating photonic structures [1–4]. The combination of these merits, along with high-quality laser crystals, allows for the construction of compact laser sources with miniaturized footprint and enhanced performance including low threshold and high efficiency [5]. Additionally, benefiting from the development of miniature pump sources in the form of diode lasers and diode-pumped solid-state lasers (DPSSLs), waveguide-based monolithic laser devices are opening up new possibilities for integrated optics.

Dual-wavelength lasers are promising for areas such as Terahertz (THz) signal generation [6–8]. Both continuous-wave (CW) and pulsed THz radiation sources show valuable applications in fields ranging from imaging, sensing and spectroscopy to communication, security and military, to give a small number of examples. $Yb^{3+}$ doped hosts have been proven to be excellent candidates as gain media for efficient lasing in the near-IR spectral range. $Yb^{3+}$ is advantageous due to its small quantum defect and high quantum efficiency [9]. In addition, Yb-doped materials possess broader absorption and emission spectra, making them particularly suitable for dual-wavelength laser generation through spectrum splitting. So far, dual-wavelength operation in a single cavity has been demonstrated with Yb-doped materials such as $Yb:GdAl_3(BO_3)_4$, Yb:YAG, Yb:LSO, $Yb:LuYSiO_5$ and Yb-doped fiber [10–14]. However, the benefits of Yb-doped hosts are often mitigated by their high lasing thresholds owing to the quasi-three-level energy diagram of Yb ions, which, as aforementioned, can be solved by utilizing highly-compact waveguide structures. $Yb:CaF_2$ waveguides fabricated by proton implantation have been previously reported [15]. Further more, dual-wavelength lasers based on phase-modulated sampled-grating waveguides fabricated in Yb-doped phosphate glass have been demonstrated [16]. Nonetheless, up till now, dual-wavelength lasers based on Yb-doped crystalline waveguides have not been reported.

Another possible solution to the above issue is to employ a host matrix that possess low photon energy which could extend the radiation lifetime of $Yb^{3+}$ ions and, hence, lower the lasing threshold. From this perspective, $CaF_2$ cubic crystal, whose photon energy is as low as $328 \text{ cm}^{-1}$ [17], turns out to be an excellent candidate and in fact, $Yb:CaF_2$ crystal has shown long emission lifetime. Additionally, $Yb:CaF_2$ crystal also possesses other advantageous properties: high thermal conductivity, high laser-induced damage threshold, low nonlinear refractive index and large transparency, making it a competitive laser material. In $Yb:CaF_2$, laser operation has been widely reported [18–22]. Furthermore, it has been demonstrated that, with non-active ions such as $Na^+$, $Y^{3+}$ or $La^{3+}$ introduced into rare-earth doped fluoride crystal, improved performance such as higher quantum efficiency can be obtained by avoiding the formation of $Yb^{2+}$-ions and, meanwhile, by breaking the ion clusters [23–28]. Su et. al. have reported diode-pumped self-Q-switched and passively mode-locked laser operation from $Yb,Na:CaF_2$ bulk crystal with single-wavelength output at 1050 nm and 1047 nm, respectively [27,28].

In this paper, we report, for the first time, on the fabrication of $Yb,Na:CaF_2$ depressed-cladding waveguides produced with ULI technology. Waveguide lasers operating in the CW and Q-switched regimes are realized with switchable single-/dual-wavelength peaking at 1013.9 nm and 1027.9 nm when pumping with a 946 nm DPSSL.

## 2. Experiments in detail

The system for the fabrication of cladding structures is depicted schematically in Fig. 1(a). The $Yb,Na:CaF_2$ crystal wafer, doped with 2.0 at% $Yb^{3+}$-ions and 5.0 at% $Na^+$-ions, is cut with the dimension of $10 \times 10 \times 2 \text{ mm}^3$ and optically polished. Using this substrate, waveguide structures that possess low-index claddings and unmodified cores are fabricated via ULI. An ultrafast Yb-doped fiber master-oscillator power amplifier laser (IMRA FCPA μ-Jewel D400), operating at a central wavelength of 1047 nm with 360 fs pulse duration and 500 kHz repetition rate is employed for waveguide fabrication. The laser beam is circularly polarized and focused beneath the sample surface ($10 \times 10 \text{ mm}^2$) through a 0.4 numerical aperture (NA) lens. The average laser power deposited on the sample is 160 mW, corresponding to a pulse energy of 320 nJ. Under these writing conditions, while the substrate is translated through the laser focus at a speed of 20 mm/s, the material properties in the focal areas are modified, inducing low-index tracks. Such a scanning procedure is repeated at different depths in the sample and, consequently, parallel tracks equally spaced around elliptic cylinders are inscribed, forming tunnel-like waveguide structures with diameters of 35 μm

(WG1, hereafter), 30 μm (WG2), 25 μm (WG3), 20 μm (WG4). These structures are positioned about 100-μm deep beneath the top surface of the sample.

The guiding properties of these waveguides are investigated by using a linearly-polarized He-Ne laser at 632.8 nm together with a typical end-face coupling arrangement. Based on the analogical coupling system, the experiments for CW and pulsed waveguide lasing are implemented by utilizing a 946 nm DPSSL as pump source. The linearly-polarized pumping laser is focused and then coupled into the waveguide through a convex lens with a focal length of 75 mm. Two dielectric plane mirrors are adhered to the waveguide facets to form a typical Fabry-Perot cavity. The input mirror gives high transmission at pumping wavelength and high reflectivity at around 1 μm, while the output mirror has reflectivity of 99% at around 946 nm and a transmittance of 20% at wavelength ranging from 1010 nm to 1070 nm. For pulsed laser generation, a two-layer graphene film coated on an optically polished sapphire wafer is used as a saturable absorber (SA), which is inserted between the output facet of the waveguide and output mirror. The thickness of sapphire layer is 1 mm with high transmittance of 85% at around 1 μm. Thus, the transmittance of output coupler for pulsed laser oscillation is considered to be 17%. The generated waveguide laser is collected by a 20 × microscope objective then characterized with detective devices.

## 3. Results and discussion
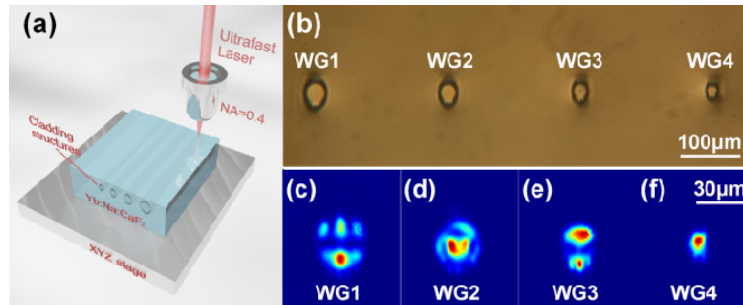


Fig. 1. (Color Online) (a) Fabrication schematic of cladding waveguides in Yb,Na:CaF$_2$ crystal with ultrafast laser.(b) The microscopic views of the output facets of cladding waveguides. (c)-(f) The measured TE mode distributions of cladding waveguides at 632.8 nm.

Figure 1(b) presents cross-sectional images of the produced waveguides observed with an optical microscope, illustrating distinct guiding boundaries without any cracks either in the waveguiding cores or in the bulk. In Fig. 1(c)-(f), the normalized near-field intensity distributions obtained under TE polarization are depicted, showing strong optical confinement. It is worthy to point out that single-mode guidance is achieved from WG4. Similar mode profiles are observed with TM-polarized laser. Moreover, the refractive index (RI) contrast between the cladding and the waveguide core is estimated by measuring NA. of the single-mode waveguide WG4, as previously introduced in Ref [7]. For both TE and TM polarizations, identical RI contrast value of $1.3 \times 10^{-3}$ is obtained, which applies to all structures produced in this work owing to the same ULI conditions. Further investigations on the propagation losses of these waveguides are performed by directly measuring the input and output laser power during end-face coupling experiment, canceling out the impacts from the Fresnel reflection of the end facets and the coupling efficiency. The propagation loss α could be estimated by the equation:

$$P_{out} = P_{in}(1-R)^2 e^{-\alpha L} T$$

where $R$ is the Fresnel reflection coefficient, $L$ is the length of the waveguide and T is the power transmission coefficient which is related to the mismatch between the pump beam

mode and waveguide mode. Assuming that the waveguides have single transmission mode which are circular in shape, $T$ could be expressed as

$$T = \left( \frac{2\omega_1\omega_2}{\omega_1^2 + \omega_2^2} \right)^2$$

in which $\omega_1$ and $\omega_2$ are the mode width of waveguide and pump beam [29]. It is found that, as waveguide diameter increases, the propagation losses decrease from 1.3 dB/cm for WG4 to 0.5 dB/cm for WG1 with slight differences along TE and TM polarizations.
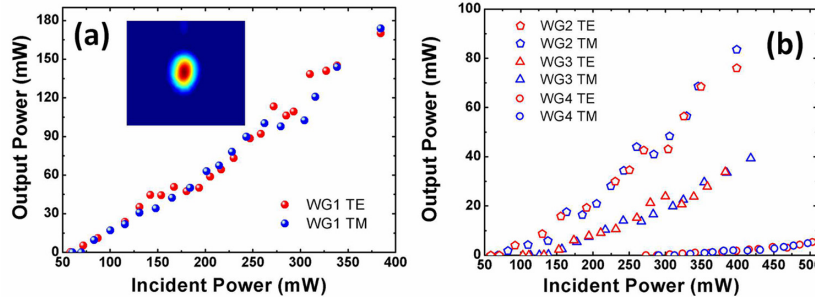


Fig. 2. The CW waveguide laser output power as a function of the incident pump power of WG1 (a) and WG2-WG4 (b). The inset of (a) shows the normalized spatial intensity distribution of the output laser mode obtained from WG1.

CW lasing is obtained from the four cladding waveguides with different performance and their powers are represented as a function of the incident pump power in Fig. 2. The best CW laser performance is achieved in WG1 with incident power threshold as low as 72.2 mW and 73.5 mW at TE and TM polarizations, respectively, as shown in Fig. 2(a). At the incident pump power of 384 mW, output power of 170 mW (TE) and 173.8 mW (TM) are achieved from WG1, giving optical-to-optical conversion efficiencies of as high as 44.3% (TE) and 45.3% (TM). The corresponding lasing modes (TE polarized) emitted from WG1 is also shown in Fig. 2(a), indicating fundamental-transverse-mode lasing. In WG2, WG3 and WG4, CW lasing operations are also achieved. As demonstrated in Fig. 2(b), WG2 give pump thresholds for laser oscillation of 96.1 mW (TE) and 105.1 mW (TM). In contrast, owing to the relatively high propagation loss, the lasing thresholds of WG4 are increased to 312.9 mW at TE and 318.2 mW at TM polarization.

The output laser is found to be switchable between single- and dual-wavelength as the pump power is varied. In WG1, when the incident pumping power is lower than 100 mW, the single-wavelength laser at 1027.9 nm is generated. In contrast, when the pumping power is higher than 220 mW, the single-wavelength laser operation at 1013.9 nm is achieved. The simultaneous dual-wavelength lasers at 1013.9 nm (peak 1) and 1027.9 nm (peak 2) are simultaneously obtained when the pumping power is changed between 100 mW and 220 mW, as evidenced by the laser emission spectra (normalized) in Fig. 3(a). The values (unit: mW) in Fig. 3(a) are corresponding to the pump powers with which the spectra are obtained. Based on the Gaussian fitting of each peak, the ratio between the integral peak 1 and peak 2 areas, A(peak 1)/A(peak 2), are determined and presented in Fig. 3(b). The spectra in Fig. 3(a) have one-to-one correspondence from left to right with the black squares marked in Fig. 3(b). As the pump power increases, the spectral intensity ratio value increases from 0.09 to 28.13, corresponding to transfer of dominance from peak 2 to peak 1. Figure 3(c) shows the laser spectra with an intensity ratio of approximately 1:1 which is obtained with 167.6 mW pump power. The FWHMs of both peaks are 3.7 nm. The center frequency difference between the two bands is determined to be 4.02 THz. Based on the intensity ratio of two peaks, the power of each peak can be calculated as a function of incident pump power, as shown in Fig. 3(d).

As can be seen, the 1013.9 nm line (peak 1) has a relatively high threshold and starts oscillation when the pump power is above 100 mW. The calculated slope efficiency is as high as 59.9%. In contrast, the 1027.9 nm line (peak 2) exhibits different behavior from the 1013.9 nm line. The output power of 1027.9 nm line increases with the pump power at first with a slope efficiency of around 46.5%, with the pump power of <146.7 mW, reaching its maximum of 31.2 mW. Then, the power decreases rapidly to around 0 when the pump power is 220 mW. Such a rapid decrease of 1027.9 nm line power can be attributed to the competition and share of gain between different energy level transitions. In WG2-WG4, such a switchable behavior of wavelength is also observed experimentally. It is worth to point out that the two wavelengths obtained in our work are very stable.
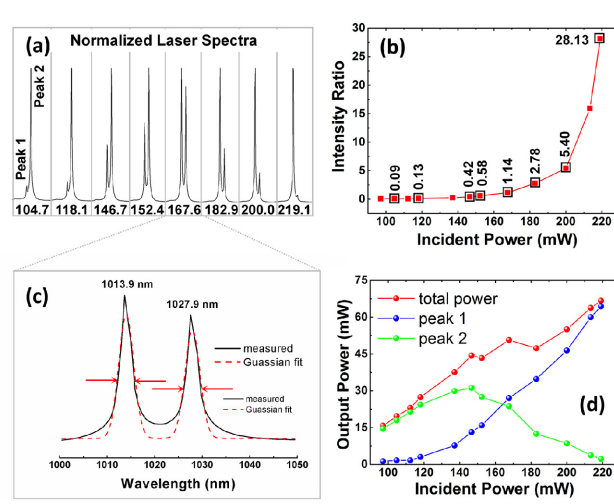


Fig. 3. (a) Normalized laser spectra of the waveguide laser in CW regime obtained under different pump powers. (b) The intensity ratio of peak 1 and peak 2 vs. the incident pump power. (c) Laser spectra with an intensity ratio of ~1:1. (d) The measured total laser (red), calculated laser power of peak 1 (blue) and peak 2 (green) as a function of incident pump power.

The luminescence emission spectrum of Yb,Na:CaF$_2$ sample used in our work is obtained with 940 nm pump source, as shown in Fig. 4, from which two emission lines corresponding the wavelengths of 1012.2 nm and 1029.9 nm can be found. These two wavelengths are in agreement with our experimental results. The origin of two wavelengths operation can be explained with the well known quasi-three-level laser model of Yb$^{3+}$ ions [30]. The energy transitions with related to these two wavelengths can be obtained, as shown in the insert of Fig. 4. Additionally, the slope efficiency for cw waveguide laser can be expressed as [31,32]

$$\eta = \frac{\ln(\frac{1}{R})}{\ln(\frac{1}{R})+2\alpha_p l} \cdot \frac{\lambda_s}{\lambda_p}[1-\exp(-\alpha_{abs}l)]\frac{dS}{dF}$$

where $R = 80\%$ is the reflectance of the output coupler, $\lambda_s$ and $\lambda_P$ are the signal and pump wavelengths, $\alpha_{abs}$ is the absorption coefficient for the pump beam, $\alpha_p$ is the propagation loss of the waveguide at the signal wavelength, $l$ is the waveguide length, and $dS/dF$ is the mode-overlap factor (i.e.,conversion efficiency of the pump light [31]). For WG1 reported in our work, it is found that when the incident pumping power is lower than 100 mW, the single-wavelength laser at 1027.9 nm is generated. Thus, the corresponding laser slope efficiency

can be estimated theoretically. For $\alpha_{abs} = 0.7$ cm$^{-1}$ [27], $\lambda_s = 1027.9$ nm and $\lambda_p = 946$ nm, the equation gives $\eta = 43\%$, which is in good agreement with the experimental results (46.5%).

By employing the two-layer graphene SA, single- and dual-wavelength operations are realized in the passively Q-switching regime from waveguides WG1, WG2 and WG3. The laser spectrum shown in Fig. 5(a) illustrates the same dual-wavelength feature as the CW laser operation. The insert of Fig. 5(a) shows the fundamental mode profile of pulsed laser achieved from WG1 with TE polarization. Figure 5(b) shows the sequence of Q-switched pulses with TE polarized pump laser. Identical pulsed trains can be obtained under TM polarization. A single laser pulse with pulse with of 500 ns is shown in Fig. 5(c). The average output power as a function of the incident pump power are shown in Fig. 5(d). The maximum output power of 26.6 mW is generated from WG1 when the incident pump power is around 400 mW. The thresholds for Q-switched laser of WG1 are 152.2 mW and 148.8 mW under TE and TM polarization, respectively. Suffering from relatively larger propagation losses, WG2 and WG3 exhibit higher lasing thresholds, which are around 250 mW and 440 mW, respectively. The average lasing slope efficiencies are determined to be around 10% for WG1, 5% for WG2, and 4% for WG3.
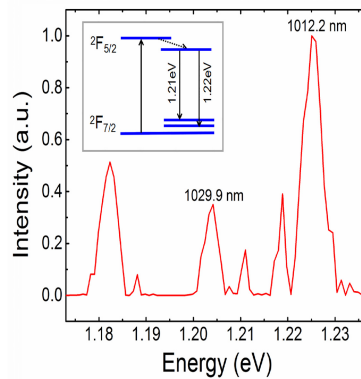


Fig. 4. The luminescence emission spectrum of Yb,Na:CaF$_2$ and energy level diagram of the Yb$^{3+}$ ions corresponding to 1012.2 nm and 1029.9 nm emissions.
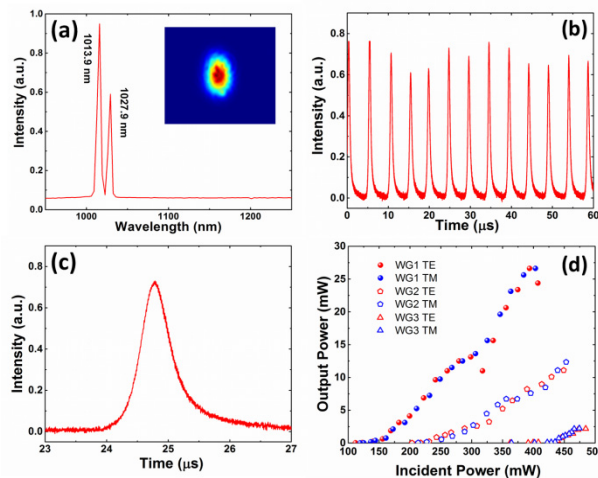


Fig. 5. (a) Spectra and fundamental mode profile of Q-switched waveguide laser obtained from WG1. (b) The sequence of Q-switched pulses. (c) A zoomed-in version of the pulse with pulse width of 500 nm. (d) The average output power as a function of the incident pump power obtained from WG1-WG3.

The repetition rate and pulse duration of Q-switched pulses generated from WG1 as a function of incident pump power are shown in Fig. 6(a). As can been seen, the repetition rates (exhibited in red) increase with the incident pump power, ranging from 49.2 kHz (104.8 kHz) to 252.0 kHz (269.3 kHz) at TE (TM) polarization. Meanwhile, the pulse duration (exhibited in blue) decreases from 177.2 ns to 103.4 ns under TE polarization and from 198.9 ns to 135.5 ns at TM polarization. The repetition rate $f_{rep}$ for passively Q-switched lasers can be expressed as [30]

$$f_{rep} = \frac{g_0}{2 \cdot \Delta R \cdot \tau_L}$$

in which $g_0$ is the small signal gain, given by $g_0 = r l_{tot}$ with $r$ being the pumping coefficient and $l_{tot}$ being the total unsaturated loss in the cavity, $\Delta R$ is the maximum modulation depth of the saturable absorber, $\tau_L$ is the upper-state lifetime. It is clear that $f_{rep}$ is proportional to the pump power. Furthermore, the pulse width $PW$ can be given by the equation [33]:

$$PW = \frac{\eta}{\rho} \frac{1}{\alpha_0 l} \frac{t_1}{\varphi_p} (r-1)$$

In this equation, $\eta$ is the energy coupling term, $\rho$ is the power coupling constant which is given by $\rho = \frac{1-R}{\sqrt{R}}$ in which $R$ is the output mirror reflectivity, $\alpha_0$ is the absorption coefficient of the unexcited laser material, $l$ is the waveguide length, $t_1$ is the cavity transit time, $\phi_p$ is peak photon flux which is given by $\varphi_p = \frac{n_{th}}{2}[r-1-\ln(r)]$ in which $n_{th}$ is the population inversion which corresponds to threshold. Therefore, it can be obtained that the pulse width is directly proportional to $\frac{r-1}{r-1-\ln(r)}$. It can be derived that $PW$ is inversely proportional to the pump power. Thus, the experiment results are in agreement with the theoretical analysis.

When the incident power is close to 453 mW, the pulse energy of WG1 Q-switched laser reaches 0.13 μJ at both TE and TM polarizations, while the peak power raise to 1.3 W (0.96 W) at TE (TM) polarization, respectively, as shown in Fig. 6(b). Furthermore, Fig. 6(b) compares the maximum pulse energy and peak power values obtained from WG1, WG2 and WG3 under fixed incident power of 430 mW, which evidenced again the best laser performance of WG1. WG2 gives a pulse energy of around 0.09 μJ and peak power approximately 0.5 W. For WG3, with the compressing of guiding core, the pulse energy and peak power are further reduced to about 0.04 μJ and 0.26 mW, respectively. Compared with the previous work [27,28], our waveguiding systems, although do not have as high output power class as that for pulsed Yb,Na:CaF$_2$ bulky laser, show prominent merits in terms of highly compacted lasing oscillation cavity, low lasing threshold and switchable single-dual-wavelength operation.
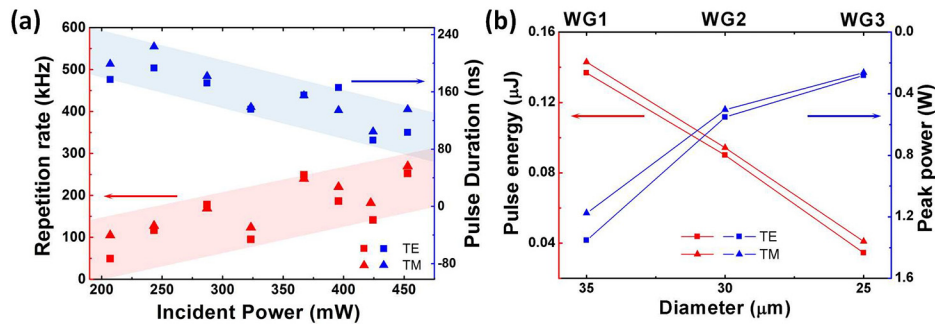
Fig. 6. (a) The repetition rate and pulse duration of Q-switched pulses generated from WG1 as a function of incident pump power. (b) Pulse energy and peak power obtained from WG1, WG2 and WG3 under fixed incident power.

## 4. Summary

In summary, we have fabricated depressed cladding waveguides in a Yb,Na:CaF$_2$ crystal by employing ULI technology. CW and graphene Q-switched waveguide lasers are realized with switchable single-dual-wavelength. The good performances of these waveguides make them promising for constructing miniature devices and integrated optical circuits for 1 μm single-dual-wavelength applications and also for lab-on-a-chip applications. In addition, these cladding structures also show their potential for mode-locked waveguide laser generation, which will be confirmed experimentally in our future works.

## Funding